Effects of Environment and Frequency on the Long Fatigue Crack Growth of Aluminium Alloy 7475

A. M. GREEN and J. F. KNOTT
Department of Materials Science and Metallurgy, University of Cambridge, Pembroke Street, Cambridge CB2 3QZ, UK

ABSTRACT

The corrosion fatigue crack growth propagation behaviour of Aluminium alloy 7475-T6 in a saltwater environment (pH3) has been investigated at a range of frequencies between 0.5 and 10Hz. The growth-rate curves in saltwater at any given frequency exhibit a sharp transition at which they tend towards that for air. The critical crack growth rate for this transition, $(da/dN)_{crit}$, is shown to be proportional to the reciprocal of the square of the loading frequency, thereby enabling an activation energy to be calculated. This is found to be consistent with that for hydrogen diffusion.

INTRODUCTION

Attempts over the past 20 years to model the corrosion fatigue (CF) behaviour of metallic materials via a Linear Elastic Fracture Mechanics (LEFM) approach have been largely based upon the interaction of the 'inert' fatigue and stress-corrosion components.

A simple superposition model has been suggested by several authors (Wei and Landes, 1969; Ford, 1979; Speidel, 1979) whereby the crack growth rates observed in CF, $(da/dN)_{CF}$ are given as the sum of those applicable to fatigue in an 'inert' environment, $(da/dN)_F$, and the equivalent terms derived from stress-corrosion data, $(da/dN)_{SCC}$. This may be represented algebraically in the form of the equation :

$$(da/dN)_{CF} = (da/dN)_F + \int (da/dt)_{SCC} \, K(t) \, dt \qquad (1)$$

This model was used with some degree of success by Speidel (1979) to predict the CF behaviour of 7079-T6, especially in the higher ΔK regime. However, this alloy exhibits stress-corrosion crack velocities two to three orders of magnitude greater than for most other 7xxx series alloys, and it would seem probable that the 'inert' fatigue contribution, $(da/dN)_F$ becomes negligible. Data obtained from other 7xxx series alloys, including 7075-T6 (Speidel, 1975; Wei *et al.*, 1980; Wei and Simmons, 1981) suggest that the simple

superposition model in the form of Equation (1) cannot account for the CF behaviour satisfactorily and that some other mechanism must be invoked.

A more recent advance on the superposition model has been proposed by Wei *et al.* (1980). Here, the CF crack growth rate is given as the sum of three components :

$$(da/dN)_{CF} = (da/dN)_F + (da/dN)_{cf} + \int (da/dt)_{SCC} K(t)dt \qquad (2)$$

where $(da/dN)_{cf}$ is a cyclic frequency dependent contribution requiring the synergistic interaction of fatigue and environment. Wei and Simmons (1981) have successfully applied this model to predict CF crack growth rates for various alloys in gaseous environments.

Investigations by Holroyd and Hardie (1983) into the changes in CF fracture mode observed in the weldable aluminium alloy 7017-T651 at certain critical crack growth rates and their dependence upon the square root of the reciprocal of the loading frequency have supported earlier suggestions that the diffusion of hydrogen ahead of the crack tip plays a significant role in CF crack growth mechanism.

In the present work, the CF crack growth behaviour of a peak-aged aluminium 7475-T6 alloy in an aerated saltwater environment has been studied, with particular emphasis placed on the effect of cyclic frequency on crack growth rates. Comparisons are drawn with previous works and the transitions from intergranular to transgranular modes of failure are related to simple diffusion models.

EXPERIMENTAL

Material

The material used throughout this study was the Al-Zn-Mg-Cu alloy 7475, containing (nominal wt%) 5.7 Zn, 2.2 Mg, 1.5 Cu, 0.2 Cr with maximum impurity cocentrations of 0.12 Fe, 0.10 Si, 0.06 Mn, 0.06 Ti. It was supplied in the form of 55mm thick rolled plate in the W51 condition. Peak hardness was achieved by a controlled increase in temperature from room temperature to 172°C at a rate of 20°C/hr and ageing in air at 172°C for 9 hrs followed by an air cool.

Material Characterisation

Specimens for optical metallography were cut from the plate in three different orientations with respect to the rolling direction. These were prepared using standard metallographic procedures and etched in Keller's reagant. Thin foil specimens for transmission electron microscope (TEM) observations were prepared from 3mm diameter bars and electropolished in a solution of 5% perchloric acid in ethanol at 20°C and at a potential of 15V. Bright field diffraction contrast imaging was used throughout to observe the alloy microstructure at high magnification.

Mechanical Testing

The testpiece design used for all fatigue testing was modified from the ASTM E399-78A compact tension specimen (CTS) to facilitate the use of a 'bolt-on' localised corrosion unit, shown in Fig.1. Specimens were machined in the ST-L orientation such that cracks would propagate along the mid-thickness plane of the plate. All testing was carried out using a computer-controlled MAND servohydraulic testing machine of 60kN capacity. Corrosion fatigue testing was conducted over a range of frequencies from 0.5 to 10Hz at ±2°C in an aerated saltwater environment containing 2.5% NaCl, 0.5% Na_2CrO_4 (acidified to pH3 using HCl). A fatigue test in laboratory air at 4Hz was also carried out to provide a means of reference. An R ratio of 0.1 and a sinusoidal waveform were used throughout. The crack length, a, was monitored via the d.c.p.d. technique and the relative crack length, a/W, was obtained from the normalised voltage, V/V_0, using a previously obtained calibration curve.

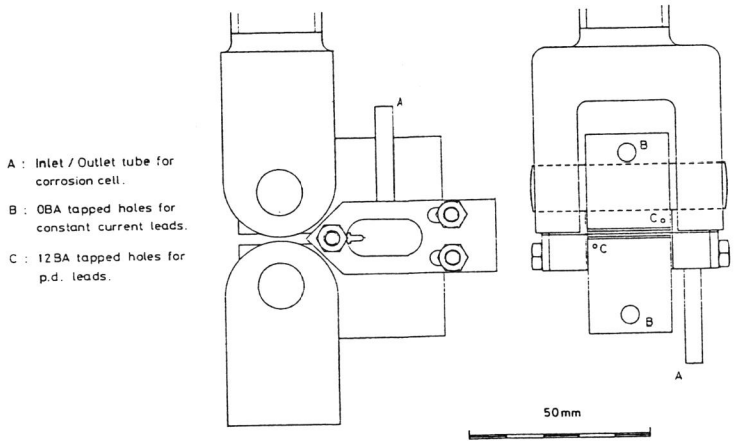

Fig. 1. Diagram showing the modified CT specimen and localised corrosion unit designs employed in corrosion fatigue testing.

Measurement of FCGR Curves

Fatigue crack growth rate (FCGR) curves were derived from the a versus N data using the 7 point incremental polynomial method. Values of the stress intensity factor range, ΔK, were calculated using the standard equation for the CTS geometry :

$$\Delta K = \frac{Y \Delta P}{B\sqrt{W}} \qquad (3)$$

where ΔP is the load range, B and W are the specimen thickness and width and Y is the appropriate compliance function (Srawley, 1976).

Fractography

The fracture surfaces of a selection of specimens were studied under the scanning electron microscope (SEM) at an operating voltage of 30kV. Particular attention was given to the fracture morphology of specimens tested in the saltwater environment in terms of cyclic frequency and crack growth rate.

EXPERIMENTAL RESULTS

Microstructure

The optical micrographs shown in Fig.2(a) illustrates the marked 'pancake' grain morphology exhibited by many cold-rolled aluminium alloys. The average diameter of the grains is approximately 100μm with a thickness of ~20μm. Fig.2(b) shows the grain structure of the L-ST orientation at a higher magnification, from which the Cr-containing grain boundary pinning particles can be seen. The main inclusions in the structure contain most of the Fe and Si impurities, and it is therefore preferable from a fracture toughness viewpoint to minimise the concentration of these elements.

The TEM microstructure around a grain boundary is shown in Fig.3. There exists a large particle size distribution, the largest approximately 100nm in diameter. The matrix strengthening precipitates are reported to be a combination of GP zones and η for the T6 temper. A narrow precipitate free zone (PFZ) can be seen around the grain boundary.

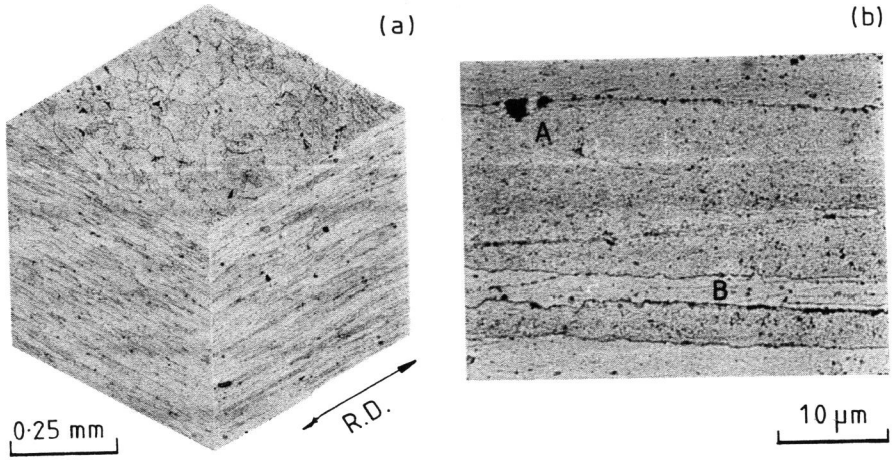

Fig. 2. Optical microstructures of alloy 7475 showing (a) a 3D representation, and (b) Fe and Si containing inclusions (A) and grain boundary pinning particles (B).

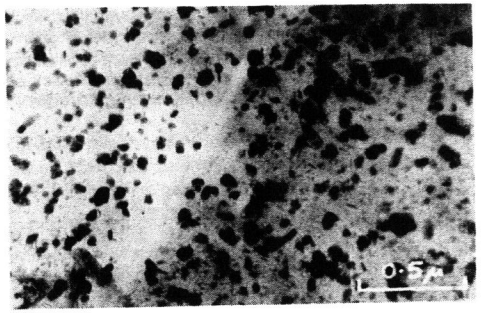

Fig. 3. TEM microstructure of alloy 7475 around a grain boundary.

Testing

The ΔK-da/dN curves obtained for tests coducted in the saline environment at 0.5, 1, 2, 4 and 10Hz, together with that for air at 4Hz are shown in Fig.4. From this graph, it is evident that at low stress intensity ranges <6 $MNm^{-3/2}$ the presence of the corrodant enhances fatigue crack propagation rates by a factor of between 5 and 6 times, although there appears to be little or no influence of loading frequency. At higher values of ΔK however, it is apparent that the CF curves deviate towards those obtained in air, and that this transition begins at lower crack growth rates as the frequency is increased.

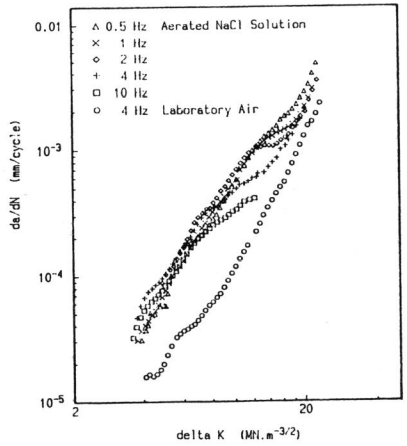

Fig. 4. Crack growth rates during fatigue of 7475 in air at 4Hz and in an aerated saltwater environment at frequencies between 0.5 and 10Hz as a function of ΔK.

Table I gives the critical crack growth rates at which deviation commences, $(da/dN)_{crit}$, for the different cyclic frequencies for specimens tested in saltwater. As K_{max} approaches the plane strain fracture toughness, K_{Ic}, the curves begin to converge irrespective of environment or loading frequency.

Table 1. Critical Crack Growth Rates for different loading frequencies.

Frequency (Hz)	$(\text{Frequency})^{-1/2}$ $(s^{1/2})$	$(da/dN)_{crit}$ (mm/cycle)
0.5	1.414	-
1	1.000	1.2×10^{-3}
2	0.707	1.0×10^{-3}
4	0.500	5.0×10^{-4}
10	0.316	2.3×10^{-4}

Fractography

Since it is now well established that the mode of failure in corrosion fatigue varies as a function of ΔK and the frequency of loading, f, it was felt that the deviations in the fatigue crack growth curves observed in Fig.4 might be accompanied by changes in fracture morphology. In general, at low ΔK and f, the fracture surfaces were flat over large areas and showed little sign of plasticity. Fig.5(a) shows the fracture surface in saltwater at 10Hz and at a ΔK of ~5 $MNm^{-3/2}$ (i.e. below $(da/dN)_{crit}$). The relatively flat region on the right is in the order of 200-300μm in size and therefore covers many individual grains.

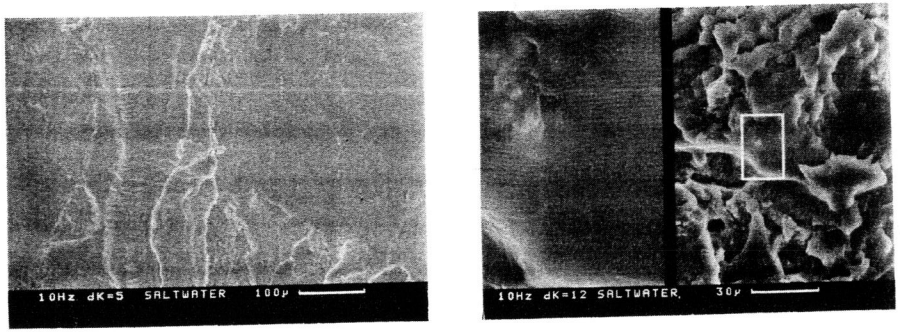

Fig. 5. SEM corrosion fatigue fracture surfaces obtained at 10Hz showing (a) flat, 'brittle' type separation at ΔK ~ 5 $MNm^{-3/2}$, and (b) ductile transgranular striations at ΔK ~ 12 $MNm^{-3/2}$.

Another prominent feature at low ΔK and f was the formation of brittle striations in strips running approximately parallel to the direction of macroscopic crack growth. The spacings between each brittle striation does not of course correspond to the amount of crack advance per cycle, and it seems most likely that they form tear-ridges linking adjacent parts of the main crack lying on different planes. At higher values of ΔK and f, the fracture mode changes to that of ductile transgranular striations, as shown in Fig.5(b). This shows marked similarities to the fatigue fracture surfaces obtained in air (Fig.6).

Unfortunately, due to the complex nature of the surfaces produced, it was extremely difficult to measure quantitatively the crack lengths at which one mode of failure gave way to another, especially as there existed a considerable variation in fracture mode across the specimen thickness. However, qualitatively, there seemed to be reasonable agreement between $(da/dN)_{crit}$ at different frequencies and the corresponding crack lengths at which fracture mode transitions were in progress.

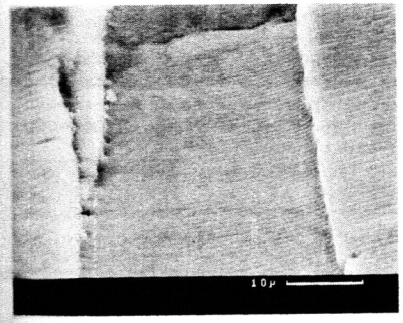

Fig. 6.

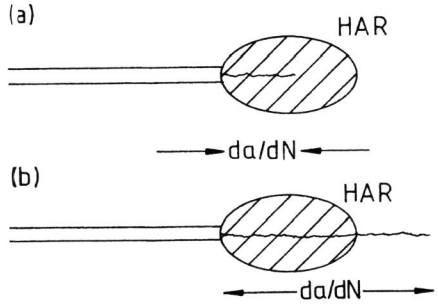

Fig. 7.

Fig. 6. SEM fatigue fracture surface of specimen tested in air at 4Hz.

Fig. 7. Schematic representation of 'nominal' crack growth rates (a) less than the Hydrogen Affected Region (HAR) size, and (b) greater than the HAR size.

DISCUSSION

From the ΔK-da/dN curves shown in Fig.4, it is possible to relate the corrosion fatigue behaviour of this material/environment system to a simple diffusion model for environmentally-assisted fatigue crack growth. At any given frequency, we may define a region ahead of the crack tip that contains a sufficient hydrogen concentration, C_H, to promote an acceleration in the rate of fatigue crack growth. Fig.7(a) shows that at 'nominal' values of da/dN less than the size of the hydrogen affected region (HAR), we would expect an increase in the amount of crack advance per cycle relative to that

in the unembrittled state. If however the FCGR is greater than the size of the HAR, as shown in Fig. 7(b), then the presence of the embrittled region will have little or no effect on da/dN. Thus we may define a critical FCGR, $(da/dN)_{crit}$, at which the transition between hydrogen-assisted and unassisted fatigue crack growth takes place.

This mechanistic model is strongly supported by the fractographic evidence provided by Figs.5(a) and 5(b), since below $(da/dN)_{crit}$, a flat, 'brittle' mode of failure is observed, whilst at higher FCGR, the ductile transgranular striations obtained closely resemble those seen in air.

A theoretical model that provides a suitable estimation of $(da/dN)_{crit}$ as a function of loading frequency may be applied to the data obtained if we assume the hydrogen concentration profile ahead of the crack to resemble that for steady state diffusion in a semi-infinite body. If this is so, then at a distance x ahead of the crack tip, the concentration of hydrogen, C_x, is given by the expression :

$$C_x = C_S \left[1 - \text{erf}\left(\frac{x}{2\sqrt{Dt}}\right)\right] = C_S \left[1 - \text{erf}\left(\frac{x}{2}\sqrt{\frac{f}{ND}}\right)\right] \qquad (4)$$

where t is the period of the loading cycle, N is the number of cycles and f the cyclic frequency. Re-arranging in terms of x gives :

$$x = \frac{2}{\sqrt{f}} \sqrt{ND}\ \text{erf}^{-1}\left(1 - \frac{C_x}{C_S}\right) \qquad (5)$$

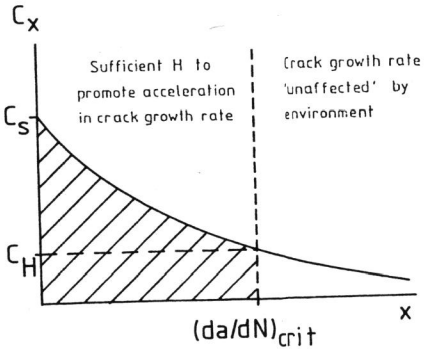

Fig. 8.

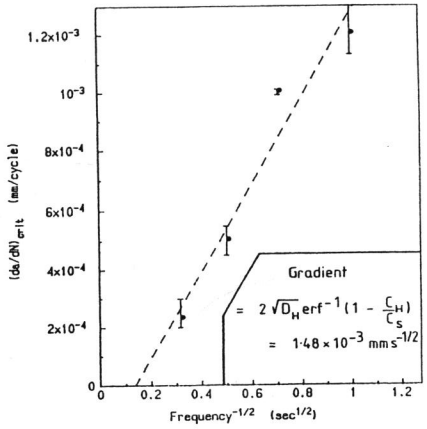

Fig. 9.

Fig. 8. Graph showing a typical hydrogen concentration profile ahead of a crack tip. The value of $(da/dN)_{crit}$ is given as the distance at which C_x is equal to C_H.

Fig. 9. Graph showing the linear dependence of $(da/dN)_{crit}$ upon $1/\sqrt{f}$.

Fig.8 shows a schematic representation of the hydrogen concentration profile ahead of the crack tip. Re-writing Equ.5 in terms of one cycle, we may substitute C_x by the minimum concentration of hydrogen required to promote an acceleration in crack growth rate, C_H, and the distance, x, by the critical crack growth rate, $(da/dN)_{crit}$, to give :

$$(da/dN)_{crit} = \frac{2}{\sqrt{f}} \sqrt{D_H}\ \text{erf}^{-1}\left(1 - \frac{C_H}{C_S}\right) \qquad (6)$$

The relationship between $(da/dN)_{crit}$ and $f^{-1/2}$ obtained from the corrosion fatigue crack growth rate curves (Fig.4) is shown in Fig.9. The linear dependence between these two variables is in good agreement with that predicted by Eq.6, from which it may be inferred that the transport of hydrogen ahead of the crack tip is the rate-controlling factor for corrosion fatigue crack growth below a certain critical rate. We may also estimate the critical hyrogen concentration ratio, C_H/C_S, although caution should be exercised, since the diffusion coefficient, D_H, will be dependant upon the diffusion path taken. However, since even in cases of transgranular failure, much of the hydrogen transport will be via the grain boundaries, then it is reasonable to assume a higher value of D_H than that for bulk diffusion. By taking 5×10^{-13} m^{2}s^{-1} as an approximation for D_H, it can be shown that C_H/C_S is in the order of 0.14. This figure is around half that reported by Holroyd and Hardie (1983), although this may be attributed to the much lower pH value of the corrodant used in this work.

CONCLUSIONS

(1) Throughout the range of frequencies tested (0.5-10Hz), the presence of the saline environment was found to cause a substantial increase in the rate of fatigue crack growth over a range of ΔK values, dependent on frequency.

(2) At low values of ΔK ($<\sim 6\text{MNm}^{-3/2}$), there is little or no effect of loading frequency on the crack growth rates observed in saltwater.

(3) For each frequency it was observed that there was a critical crack growth rate, above which the ΔK-da/dN curve deviated from the previous linear form, towards the curve for the air environment.

(4) A model has been proposed whereby the dependence of the critical crack growth rate, $(da/dN)_{crit}$, upon the square root of the reciprocal of the loading frequency, $1/\sqrt{f}$, has been attributed to the steady-state diffusion of hydrogen ahead of the crack tip. This model is consistent with the observed values.

(5) SEM observations tend to confirm suggestions that transitions in the growth rate curves for specimens tested in saltwater are accompanied by changes in fracture mode from one of brittle nature at low ΔK and f, to ductile transgranular striations at higher ΔK and f.

(6) By taking a value for the grain boundary diffusion coefficient of H in Al of 5×10^{-13} m^{2}s^{-1}, a critical hydrogen concentration ratio to promote accelerated fatigue crack growth, C_H/C_S of 0.14 has been obtained.

ACKNOWLEDGEMENTS

Professor D.Hull is thanked for the provision of laboratory facilities. The financial support given by Alcan International Limited and by the Science and Engineering Research Council is also gratefully received.

REFERENCES

American Society for Testing and Materials Standard E399-78A (1979). In: *1979 Annual Book of ASTM Standards*, Part 10, 540.
Ford, F.P. (1979). *Corrosion*, **35**, 281.
Holroyd, N.J.H. and Hardie, D. (1983), *Corros. Sci.*, **23**, 527.
Speidel, M.O. (1975), *Metall. Trans.*, **6A**, 631.
Speidel, M.O. (1979). In: *Stress Corrosion Research* (ed. Arup and Parkins), NATO, Sijthoff and Norrdhoff, 117.
Srawley, J.E. (1976), *Int. J. Fract.*, **12**, 475.
Wei, R.P. and Landes, J.D. (1969), *Mater. Res. Standards*, **9**, 25.
Wei, R.P., Pao, P.S., Hart, R.G., Weir, T.W. and Simmons, G.W. (1980), *Metall. Trans.*, **11A**, 151.
Wei, R.P. and Simmons, G.W. (1981), *Int. J. Fract.*, **17**, 235.